Initial Attempt on Outdoor Human Detection using IEEE 802.11ac WLAN Signal

Masahiko Miyazaki*, Shigemi Ishida*, Akira Fukuda*, Tomoki Murakami†, Shinya Otsuki†
*ISEE, Kyushu University, Fukuoka 819-0395, Japan
{miyazaki, ishida, fukuda}@f.ait.kyushu-u.ac.jp
†Access Network Service Systems Laboratories, NTT Corporation, Kanagawa 239-0847, Japan
{murakami.tomoki, Otsuki.Shinya}@lab.ntt.co.jp

***Abstract*—In recent years, the functionality of wireless communications has not only been limited to communication between users, but has also been extended to sensing applications. In fact, several WLAN-based sensing technologies, which rely on changes in multipath radio propagation derived from a channel state information (CSI) in indoor environments, have already been developed. In this paper, we present a WLAN-based outdoor human detection system – the first in IEEE 802.11ac WLAN CSI-based outdoor sensing attempts. The number of multipaths in an outdoor environment is limited, thus, making sensing difficult. To realize outdoor CSI sensing, we present an IEEE 802.11ac WLAN-based sensing system. Specifically, this paper tries to answer the question, *"How do we install a transmitter-receiver pair?"* based on an analysis of the experimental results. Moreover, we provide open discussions regarding the optimum installation of WLAN sensing devices.**

***Index Terms*—WLAN sensing, channel state information (CSI), outdoor, human detection.**

I. Introduction

In recent years, the functionality of wireless communications has been extended to incorporate sensing applications, aside from communication between users. Wireless sensing technologies rely on changes in radio signals caused by sensing target objects. The prevalence of wireless local area networks (WLANs) these days is undeniable. WLAN devices already deployed in the environments can be utilized for sensing without additional equipments.

WLAN sensing technologies utilize received signal strength (RSS) for sensing. RSS partially reflects the changes in radio signals and is eligible to detect changes of target objects around the radio signal paths. A couple of papers have been presented outdoor WLAN sensing technologies based on RSS such as [1].

Recently, more precise WLAN sensing approaches have also been proposed employing channel state information (CSI), a radio path model between a transmitter and a receiver first defined in IEEE 802.11n. The CSI includes amplitude and phase information for each orthogonal frequency division multiplexing (OFDM) subcarrier, originally designed for beamforming. Multipath fading is dependent on these subcarriers whose frequencies are slightly different. WLAN sensing technologies analyze the CSI to extract changes in the multipath for sensing, such as object detection and object movement recognition.

Many CSI-based sensing methods have already been proposed including Smokey, TensorBeat, and SafeDrive-Fi [2]–[8]. These methods analyze CSI and successfully realize accurate sensing in indoor environments, using machine learning classifiers.

However, CSI-based WLAN sensing is difficult in an outdoor environment because of small differences in the multipath for each subcarrier and a very limited number of multipaths in such environment. In addition, radio signals from the line-of-sight (LOS) path also make it difficult, or sometimes prevent, the observation of small changes in the multipath environment.

To realize CSI-based outdoor sensing, this paper presents an IEEE 802.11ac WLAN-based sensing system. The idea is to utilize multiple transmitter-receiver pairs to reduce the sensing target area covered by each pair. We installed several WLAN devices in a sensing target area and performed sensing using a sufficient amount of CSI derived from the multiple transmitter-receiver pairs. We employed the CSI collection system presented in our previous study to efficiently collect CSI from IEEE 802.11ac sound-protocol-compliant transmitter-receiver pairs [9]. Moreover, we developed a human detection system example of the WLAN-based sensing, and also conducted discussions on the deployment of WLAN sensing devices. Specifically, we accomplished these three objectives in this study:

- Design of an IEEE 802.11ac WLAN-based outdoor human detection system that collects CSI data from multiple transmitter-receiver pairs. To the best of our knowledge, this is the first, explicit attempt for an outdoor sensing using IEEE 802.11ac WLAN CSI.
- Basic detection performance assessment of the outdoor human detection system through experimental evaluations using actual IEEE 802.11ac devices.
- Open discussions regarding the installation of transmitter-receiver pairs to improve the system's performance.

The remainder of the paper is structured as follows. Section II discusses an existing CSI-based indoor human sensing method. Section III outlines the proposed outdoor human detection system. Section IV provides the results of the evaluation experiment conducted for the proposed system, along with discussions on its installation, and Section V concludes the paper.

II. Related Works

To the best of our knowledge, the IEEE 802.11ac WLAN sensing is a novel CSI-based outdoor sensing technology. In this section, we will discuss WLAN-based indoor sensing technologies.

doi: 10.1109/SAS.2019.8706126

One of the sources of WLAN-based sensing is the fluctuation characteristics of the received signal strength (RSS) [6], [10]–[13]. Kosba et al. proposed a localization system named RASID using WLAN RSS [10]. They combined the RSS from multiple nodes and estimated a human location using a statistical anomaly detection technology. Abdlelnasser et al. proposed a gesture recognition system named WiGest [5], [6], which consists of primitive extraction, gesture identification, and action mapping. Although RSS is one of the easiest sources in WLAN sensing systems, an unsteady RSS possesses limited capabilities to describe environmental changes, resulting in low sensing performance of the device.

CSI consists of amplitude and phase information of each OFDM subcarrier, and is known to have more fine-grained information than the RSS [14]. Thus, CSI is used in several WLAN sensing methods in the recent years [2]–[4], [7], [8], [15]–[19]. Y.Wang et al. proposed a location-oriented activity identification system named E-eyes [15], capable of estimating the location of a walking user by Dynamic Time Wrapping (DTW) and associating CSI with specific activities by Earth Mover Distance (EMD). W.Wang et al. proposed a human activity recognition system named CARM [16], [17], which consists of a CSI speed model that estimates motion for each part of the body, and a CSI activity model that combines the body parts speed information with specific actions by using a hidden Markov model (HMM). Zheng et al. proposed a ubiquitous smoking detection system named Smokey [2] that extracts motion from CSI using a foreground detection technology used in the image processing community, and detects continuous smoking activity using autocorrelation. X.Wang et al. proposed a multi-person breathing beats monitoring system named TensorBeat [3], which creates tensor data from CSI phase difference and designs a matching algorithm to distinguish individuals. Arshad et al. proposed a dangerous driving detection system named SafeDrive-Fi [4] that uses an EMD to retrieve human behavior from noisy CSI data and classifies driver status using k-Nearest Neighbor (kNN) or Support Vector Machine (SVM) unsupervised learning. Ali et al. proposed keystroke recognition system named WiKey [18], [19], in which noise components are first removed from CSI by using low pass filter and principal component analysis (PCA), and then feature quantities are extracted using discrete wavelet transformation (DWT). A model is then created for all keys based on these feature quantities, and identification is performed using kNN.

Because CSI includes a large amount of information, deep-learning-based approaches have also been proposed. Feng et al. proposed activity detection systems using a Long Short-Term Memory (LSTM), a type of Recurrent Neural Network (RNN) [7], to achieve highly accurate and efficient activity recognition. Chen et al. proposed a passive human activity recognition system using attention-based bi-directional LSTM [8], by utilizing a learning network that analyzes time changes in two directions for higher performance. The sensing methods described above use the CSI derived in a 20-MHz band specified in IEEE 802.11n, which is acquired with Linux 802.11n CSI Tool [20].

Prior to this research, we have developed a CSI acquisition system using IEEE 802.11ac [9] that efficiently collects CSI data from multiple wireless links in target areas thru installation of multiple CSI measuring stations. The CSI monitoring station captures all wireless packets transmitted within the communication range and extracts the CSI by analyzing the packet based on the sounding protocol specified in IEEE 802.11ac. Thus, extending the sensing target area is possible through installation of multiple measuring stations. This paper adopts the above CSI acquisition system for human detection in a specified target area.

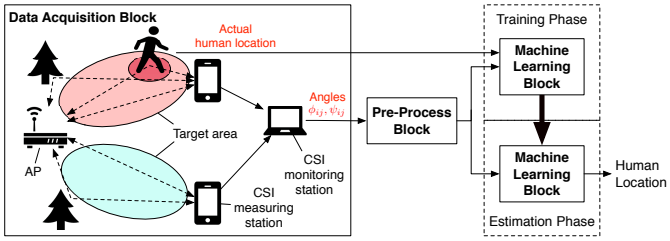

Fig. 1. Overview of IEEE 802.11ac WLAN-based outdoor human detection system

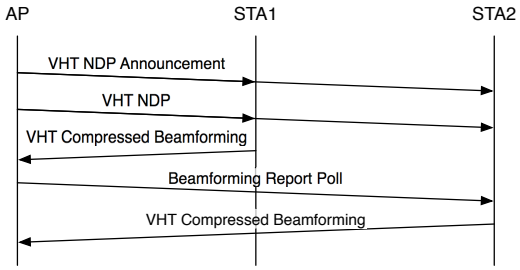

Fig. 2. Communication sequence example of VHT sounding protocol in IEEE 802.11ac

III. IEEE 802.11ac WLAN-based Outdoor Human Detection System

A. Design Overview

Figure 1 shows an overview of the IEEE 802.11ac WLAN-based outdoor human detection system. The detection system consists of data acquisition, pre-process, and machine learning blocks. In data acquisition block, we collect the CSI data from multiple transmitter-receiver pairs. The pre-process block denoises and normalizes the CSI data, which is then passed to the machine learning block to detect a human and his/her location.

The subsequent subsections describe the three blocks in detail.

B. Data Acquisition Block

Figure 1 shows the data acquisition block, which consists of a WLAN access point (AP), CSI measuring stations, and a CSI monitoring station. The data acquisition block retrieves the CSI data using the very high throughput (VHT) sounding protocol defined in IEEE 802.11ac standards [21].

Figure 2 depicts a communication sequence example of the VHT sounding protocol in case that an AP retrieves

TABLE I
RELATIONSHIP BETWEEN ANGLES ϕ_{ij}, ψ_{ij} AND THE SIZE OF CSI FEEDBACK MATRIX

Size of CSI feedback matrix	Number of angles	The order of angles in beamforming frames
2×1	2	ϕ_{11}, ψ_{21}
2×2	2	ϕ_{11}, ψ_{21}
3×1	4	ϕ_{11}, ϕ_{21}, ψ_{21}, ψ_{31}
3×2	6	ϕ_{11}, ϕ_{21}, ψ_{21}, ψ_{31}, ϕ_{22}, ψ_{31}
3×3	6	ϕ_{11}, ϕ_{21}, ψ_{21}, ψ_{31}, ϕ_{22}, ψ_{31}
4×1	6	ϕ_{11}, ϕ_{21}, ϕ_{31}, ψ_{21}, ψ_{31}, ψ_{41}
4×2	10	ϕ_{11}, ϕ_{21}, ϕ_{31}, ψ_{21}, ψ_{31}, ψ_{41}, ϕ_{22}, ϕ_{32}, ψ_{32}, ψ_{42}
$\vdots$	$\vdots$	$\vdots$

CSI from two stations. An AP initiates the VHT sounding by broadcasting a `VHT null data packet (NDP) announcement` frame. The AP then periodically broadcasts a `VHT NDP` frame that includes training symbols to estimate a CSI. Stations receive the `VHT NDP` frame and estimate the CSI, which is compressed into angle information described by $\phi_{ij} \in [0, 2\pi]$ and $\psi_{ij} \in [0, \pi/2]$ using Givens rotation. One of the stations sends a `VHT compressed beamforming` frame including ϕ_{ij} and ψ_{ij} to the AP. The other station waits for a `beamforming report poll` frame before sending a `VHT compressed beamforming` frame to the AP.

A CSI monitoring station captures the `VHT compressed beamforming` frames sent from stations. The compressed angles ϕ_{ij} and ψ_{ij} are extracted and passed to a pre-process block.

The compressed angles ϕ_{ij} and ψ_{ij} represent relative phase and amplitude difference between antennas, respectively [22]. The angle ϕ_{ij} and ψ_{ij} are quantized with specific bits b_ϕ and b_ψ, respectively. $b_\phi \in \{4, 6, 7, 9\}$ and $b_\psi \in \{2, 4, 5, 7\}$ are specified in the header of a `VHT compressed beamforming` frame depending on feedback type. Thus, for a single-user feedback type, $[b_\phi \ b_\psi] \in \{[4\ 2], [6\ 4]\}$.

The angles ϕ_{ij} and ψ_{ij} are described as

$$\phi_{ij} = \frac{k\pi}{2^{b_\phi - 1}} + \frac{\pi}{2^{b_\phi}}, \quad \text{where } k = 0, 1, \ldots, 2^{b_\phi} - 1, \tag{1}$$

$$\psi_{ij} = \frac{l\pi}{2^{b_\psi + 1}} + \frac{\pi}{2^{b_\psi + 2}}, \quad \text{where } l = 0, 1, \ldots, 2^{b_\psi} - 1. \tag{2}$$

The number of angles, i.e., $|\{\phi_{ij}\}|$ and $|\{\psi_{ij}\}|$, depends on the size of a CSI feedback matrix. Table I shows the relationship between the size of CSI feedback matrix and the number of angles, as well as their order in `VHT compressed beamforming` frames. We derived at least $52 \times (|\{\phi_{ij}\}| + |\{\psi_{ij}\}|)$ angle information from each beamforming frame because the IEEE 802.11ac uses 52 (+ 4 pilot) subcarriers in a 20-MHz VHT mode.

C. Pre-Process Block

The pre-process block applies a filter to reduce environmental noise and normalize the angle information ϕ_{ij} and ψ_{ij}.

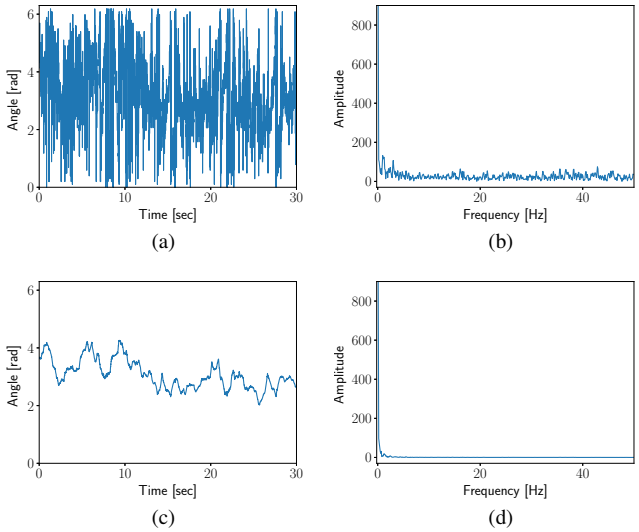

Fig. 3. Example of angle ϕ_{11} with human in a target area: (a) raw data, (b) FFT result for raw data, (c) filtered data, and (d) FFT result for filtered data

In outdoor environments, radio propagation is highly affected by slight changes in objects such as sway of trees, which results in noisy angle data. Figure 3a shows a typical example of the noisy angle data. The figure shows actual angle data ϕ_{11} of subcarrier -28 with a human walking in a target area. Figure 3b shows the fast Fourier transform (FFT) result of the ϕ_{11} data. Note that the frequency components of the walking motion are less than 4 Hz [23]. High-frequency components indicate environmental noise other than the influence of human motion.

The pre-process block applies a low-pass filter (LPF) to reduce the influence of environmental noise. We used a simple moving-average LPF. Based on our preliminary experiment results, we applied a moving average over one second.

Figures 3c and 3d show an example of the filtered angle data and its FFT result derived from angle data in Fig. 3a. In these figures, high frequency environmental noise is reduced while the low frequency components are preserved. We then used the filtered output in the machine learning block.

We normalized the angle data ϕ_{ij}, ψ_{ij} before passing them to the machine learning block for better performance. This is done, because machine learning algorithms suffer from performance degradation, including long training time and decrease in accuracy, with different scale features.

As described in III-B, the range of ϕ_{ij} and ψ_{ij} are $\phi_{ij} \in [0, 2\pi]$ and $\psi_{ij} \in [0, \pi/2]$, respectively. The normalized angles $\hat{\phi}_{ij}$ and $\hat{\psi}_{ij}$ are defined as

$$\hat{\phi}_{ij} = \frac{1}{2\pi}\phi_{ij}, \tag{3}$$

$$\hat{\psi}_{ij} = \frac{2}{\pi}\psi_{ij}. \tag{4}$$

D. Machine Learning Block

The machine learning block detects a human as a classification task. We did not put a limit on the classification methods. For instance, if we use multi-label classifier, the human

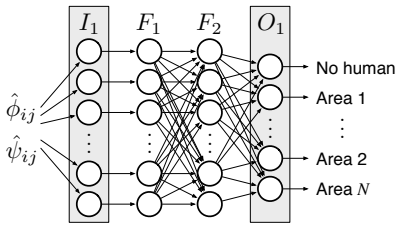

Fig. 4. DNN architecture in machine learning block

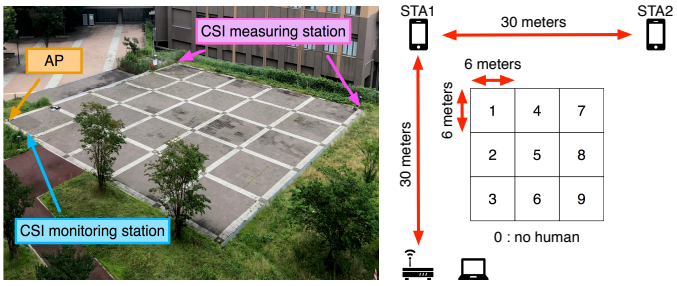

Fig. 5. Experiment setup

detection system is capable of area detection by estimating the approximate location of the detected human. Therefore, we employed the deep neural network (DNN)-based multi-label classifier for this study.

Figure 4 shows the DNN architecture in the machine learning block. The DNN network consists of an input layer, two hidden layers, and a softmax output layer. The network process is as follows. First, the DNN architecture takes normalized angles $\hat{\phi}_{ij}, \hat{\psi}_{ij}$ as input to an input layer I_1. Next, the input data is directly passed to two fully connected layers F_1, F_2. The number of units in F_1, F_2 is therefore set to the number of angles $52 \times (|\{\phi_{ij}\}| + |\{\psi_{ij}\}|)$. Finally, the standard softmax function is employed in an output layer O_1. The number of outputs is identical to the number of detection target states: the number of areas plus one.

In the training phase, the DNN was tasked in multi-label classification by employing the standard back-propagation with the Adam gradient method [24], for a mini-batch size of 512. The Keras/TensorFlow framework with the Dropout [25] and Early Stopping [26] techniques were employed in our experiments.

IV. Evaluation

To assess the basic performance of our WLAN-based outdoor sensing system, we conducted experimental evaluations in an outdoor environment at the Kyushu University.

A. Experiment Setup

Figure 5 shows the setup of the experiment. We installed a testbed WLAN AP and two Galaxy S7 edge CSI measuring stations, denoted as STA1 and STA2 in the right side of the figure, in an open space. No obstacle was permitted between the AP and the CSI measuring stations. An Intel Compute Stick STK2m364CC CSI monitoring station was also installed near the AP. With these devices, we derived 4×1 CSI feedback matrix and acquired 312 angle information (= 6 angles $\times$52 subcarriers).

The AP and CSI measuring stations were installed at corners of a 30-meter grid, at a height one meter from the ground (Fig. 5).

The CSI monitoring station was installed on the ground near the AP. Moreover, we used WLAN channel 100 in a 5-GHz band.

We divided the detection target area into nine 6-meter square areas labeled from `1` to `9`, as shown in Fig. 5. The CSI data, i.e., angle information ϕ_{ij}, ψ_{ij}, was collected at a sampling rate of 100 Hz for 60 seconds while a human is randomly walking in each area. We also collected the CSI data for a target area without a human, and labeled it as area `0`. For STA1 and STA2, the average numbers of CSI data acquired in each area were 5,959 and 5,608, respectively. Using the collected data, our detection system was able to detect a human and his/her location in the target area.

TABLE II
Human Detection Performance

	STA1	STA2
Number of TPs	4,077,622	4,919,199
Number of FNs	859,378	314
Number of FPs	344,904	201
Precision	92.20	99.99
Recall	82.59	99.99
$\mathrm{F}_{\mathrm{measure}}$	87.13	99.99

B. Detection Performance

We evaluated the detection performance of our outdoor human detection system with the following process. First, we divided the CSI data into *with-human* and *without-human* classes corresponding to labels `1` to `9` and label `0`, respectively. To equalize the amount of training/testing data in the two classes, we randomly over-sampled the *without-human* data. Next, we trained the DNN model presented in Section III-D as a binary classifier and performed 10-fold leave-one-out cross validation for 100 trials with an initialized classifier model in each trial. Finally, we counted the number of true positives (TPs), false positives (FPs), and false negatives (FNs) by summing the results for all the trials. We also calculated the precision, recall, and F-measure of the data.

Table II shows the results of the detection performance evaluation. For STA1, our human detection system successfully detected the human target with an F-measure of 87.13 %. The recall was 82.59 % due to several FN detections. In some areas far from a wireless link between TX and STA1, the system failed to detect human due to small changes in the CSI data resulting from multiple FNs. For STA2, our detection system showed almost perfect detection accuracy. From these results, we showed that CSI could monitor environmental changes in a limited area, restricted by the surrounding environment and the distance between the CSI monitoring equipment.

C. Area Estimation Performance

We evaluated the area estimation performance of our human detection system according to the following procedures. First,

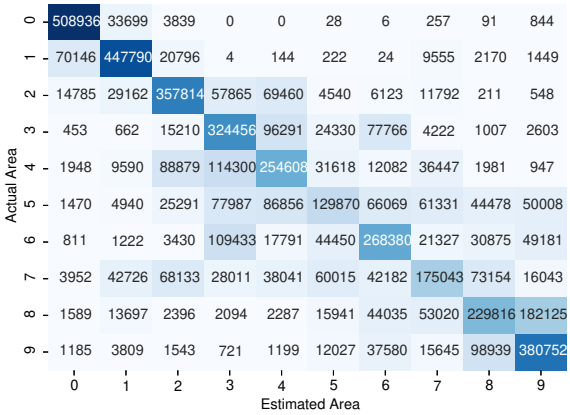

Fig. 6. Confusion matrix with the result of STA1

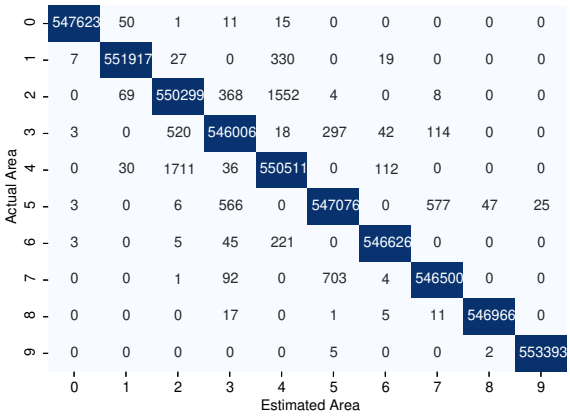

Fig. 7. Confusion matrix with the result of STA2

the DNN model was re-trained using the data with labels 0 to 9 as a 10-class classifier to estimate an area where a human can be located. We performed a 10-fold leave-one-out cross validation for 100 trials with an initialized classifier model in each trial and generated a confusion matrix.

Figures 6 and 7 show the confusion matrices of area detection results derived from the CSI data of STA1 and STA2, respectively. Each cell in the matrices represents the number of detection results in the estimated area, represented in columns, and by the actual area, represented in rows. The total accuracies with STA1 and STA2, i.e., ratio of the sum of diagonal elements to the sum of all elements in the matrices, were 56.01 % and 99.86 %, respectively.

From Fig. 6, the detection accuracies for areas 0 to 3 and 9 were 92.92 %, 81.08 %, 64.79 %, and 68.80 %, respectively, which are higher compared to the other areas. The accuracy for area 5 was significantly low at 23.68 %. The presence of a human highly affected the communication signals in areas 1 to 3 as these areas were located near the AP and STA1, as

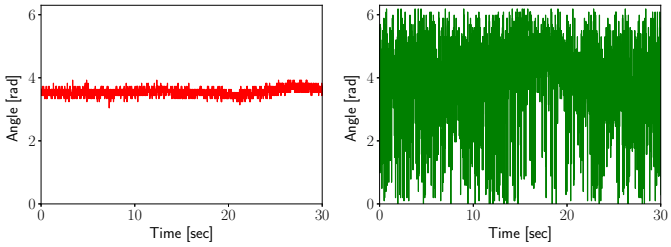

Fig. 8. Example of ϕ_{11} of subcarrier -27 in area 0 derived from (a) STA1 and (b) STA2

depicted in Fig. 5. For area 9, the presence of trees created multipaths between AP and STA1, which might have caused high detection accuracy in the area.

For area 0, we also realized some fluctuations in the CSI if a human was present in any one of the areas 1–9. For area 5, which is adjacent to all other areas except area 0, the accuracy was degraded due to fluctuations in the CSI similar to the pattern observed for the other areas.

Thus, as shown in Fig. 7, we could perform estimation of the 10 areas with high accuracies from STA2. In this experiment setup, we could derive CSI changes sufficient to estimate an area, where a human is present, from the data derived with a human walking in each area.

D. Discussion on Installation Environment

Our experimental results indicated that the locations of AP and STA and their surrounding environment have great influence on detection range and accuracy. Optimizing the installation is therefore an important task in sensing with WLAN signals in an outdoor environment.

Fluctuations in CSI greatly differ between STA1 and STA2. Figure 8 shows the raw ϕ_{11} value of subcarrier -27 as a function of time retrieved from STA1 and STA2 in area 0, i.e. with no human in any area. From the figure, the ϕ_{11} of STA2 clearly shows larger variation than that of STA1. The same trend was observed in other angle information. Thus, the large fluctuation indicates that the sensitivity of the CSI to the change in environment is high. This clarifies the high detection performance derived with STA2.

We also believe that signal-to-noise ratio (SNR) is one of the factors related to CSI fluctuations. Figure 9 shows the SNR given to the CSI reporting frames. Note that the SNR of the link between TX and STA1 was higher than that of the link between TX and STA2 by more than 10 dB. In general, WLAN network interface cards (NICs) are designed to demodulate received signals above a certain strength based on SNR. As SNR decreases, weak signals are more amplified in a radio circuit and are demodulated. Environmental changes are observed as changes in multipaths, from which the weak radio signals are received. Therefore, the small SNR in STA2, with constant noise level, causes higher amplifier gain, resulting to higher detection performance derived with amplified multipath information.

In our experiment setup, difference in distance between the AP and the STA highly affected the detection performance.

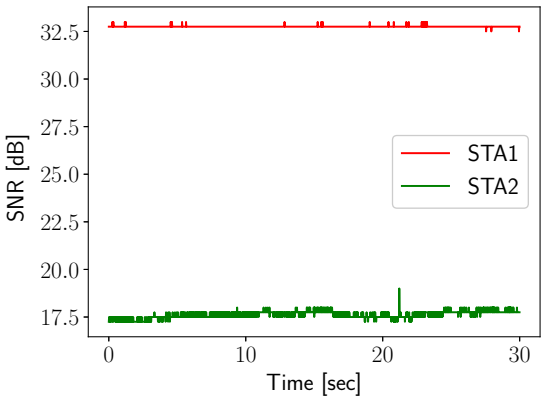

Fig. 9. Example of signal to noise ratio (SNR) in area 0 derived from STA1 and STA2

SNR decreases as the distance gets longer because radio signals are attenuated proportionally to the inverse of the square of the distance. Thus, the increase in propagation distance results in smaller power differences between signals from a direct path and multipaths although the received signal strength decreases. The locations of TX and STA might be another cause of the difference in SNRs, which is difficult to prove.

To improve detection performance, these three approaches might help: (a)Reduction of transmission power. Small transmission power forces receivers to amplify the received signal, which could reveal good performance as discussed above. (b) Installation of AP and STA in a non-line-of-sight (NLOS) environment. By blocking a direct path (which is less affected by changes in the environment) between the AP and the STA, we can emphasize the influence of environmental changes on the received signals. (c) Sensing with wider bandwidth. By adopting channel bonding, much more amount of CSI can be acquired, which might help the proposed system to detect a human. Further investigation is required to confirm the implications of these approaches.

V. Conclusion

In this paper, we presented a WLAN-based human detection system, the first of attempts for an outdoor sensing using IEEE 802.11ac WLAN CSI, where the number of multipaths is very limited. We extracted beamforming angle information from IEEE 802.11ac nodes and estimated human presence by employing deep neural network (DNN). Through experimental evaluations, we validated that with a specific setup, the system can detect human presence as well as estimate his/her location with high accuracy of 99.86 %.

Acknowledgment

This work was supported in part by JSPS KAKENHI Grant Numbers JP15H05708 and JP18K18041.

References

[1] S. Depatla, A. Muralidharan, and Y. Mostofi, "Occupancy estimation using only WiFi power measurements," *IEEE J. Sel. Areas Commun.*, vol. 33, no. 7, pp. 1381–1393, Jul. 2015.

[2] X. Zheng, J. Wang, L. Shangguan *et al.*, "Smokey: Ubiquitous smoking detection with commercial wifi infrastructures," in *Proc. IEEE Int. Conf. on Computer Communications (INFOCOM)*, Jul. 2016, pp. 1–9.

[3] X. Wang, C. Yang, and S. Mao, "TensorBeat: Tensor decomposition for monitoring multiperson breathing beats with commodity WiFi," *ACM Trans. Intelligent Systems and Technology (TIST)*, vol. 9, no. 1, pp. 1–27, Sep. 2017, article No.8.

[4] S. Arshad, C. Feng, I. Elujide *et al.*, "SafeDrive-Fi: A multimodal and device free dangerous driving recognition system using WiFi," in *Proc. IEEE Int. Conf. on Communications (ICC)*, May 2018, pp. 1–6.

[5] H. Abdelnasser, M. Youssef, and K. A. Harras, "WiGest: A ubiquitous WiFi-based gesture recognition system," in *Proc. IEEE Int. Conf. on Computer Communications (INFOCOM)*, Apr.–May 2015, pp. 1–9.

[6] H. Abdelnasser, K. A. Harras, and M. Youssef, "A ubiquitous WiFi-based fine-grained gesture recognition system," *IEEE Trans. Mobile Comput.*, pp. 1–14, Nov. 2018, early access.

[7] C. Feng, S. Arshad, R. Yu *et al.*, "Evaluation and improvement of activity detection systems with recurrent neural network," in *Proc. IEEE Int. Conf. on Communications (ICC)*, May 2018, pp. 1–6.

[8] Z. Chen, L. Zhang, C. Jiang *et al.*, "WiFi CSI based passive human activity recognition using attention based BLSTM," *IEEE Trans. Mobile Comput.*, pp. 1–12, Oct. 2018, early access.

[9] T. Murakami, M. Miyazaki, S. Ishida *et al.*, "Wireless LAN based CSI monitoring system for object detection," *MDPI Electronics*, vol. 7, no. 11, pp. 1–11, Nov. 2018, article no.290.

[10] A. E. Kosba, A. Saeed, and M. Youssef, "RASID: A robust WLAN device-free passive motion detection system," in *IEEE PerCom*, mar 2012, pp. 1–10.

[11] M. Seifeldin, A. Saeed, A. E. Kosba *et al.*, "Nuzzer: A large-scale device-free passive localization system for wireless environments," *IEEE Trans. Mobile Comput.*, vol. 12, no. 7, pp. 1321–1334, Jul. 2013.

[12] Y. Shu, Y. Huang, J. Zhang *et al.*, "Gradient-based fingerprinting for indoor localization and tracking," *IEEE Trans. Ind. Electron.*, vol. 63, no. 4, pp. 2424–2433, Apr. 2016.

[13] T. Wei, S. Wang, A. Zhou *et al.*, "Acoustic eavesdropping through wireless vibrometry," in *Proc. ACM MobiCom*, Sep. 2015, pp. 130–141.

[14] J. Xiao, Z. Zhou, Y. Yi *et al.*, "A survey on wireless indoor localization from the device perspective," *ACM Computing Surveys (CSUR)*, vol. 49, no. 2, pp. 1–31, Jun. 2016, article no.25.

[15] Y. Wang, J. Liu, Y. Chen *et al.*, "E-eyes: Device-free location-oriented activity identification using fine-grained WiFi signatures," in *Proc. ACM MobiCom*, Sep. 2014, pp. 617–628.

[16] W. Wang, A. X. Liu, M. Shahzad *et al.*, "Understanding and modeling of WiFi signal based human activity recognition," in *Proc. ACM MobiCom*, Sep. 2015, pp. 65–76.

[17] W. Wang, A. X. Liu, M. Shahzad *et al.*, "Device-free human activity recognition using commercial WiFi devices," *IEEE J. Sel. Areas Commun.*, vol. 35, no. 5, pp. 1118–1131, May 2017.

[18] K. Ali, A. X. Liu, W. Wang *et al.*, "Keystroke recognition using WiFi signals," in *Proc. ACM MobiCom*, Sep. 2015, pp. 90–102.

[19] K. Ali, A. X. Liu, W. Wang *et al.*, "Recognizing keystrokes using WiFi devices," *IEEE J. Sel. Areas Commun.*, vol. 35, no. 5, pp. 1175–1190, May 2017.

[20] D. Halperin, W. Hu, A. Sheth *et al.*, "Tool release: Gathering 802.11n traces with channel state information," *ACM SIGCOMM Computer Commun. Review (CCR)*, vol. 41, no. 1, p. 53, Jan. 2011.

[21] IEEE Standards Association, "IEEE Std 802.11-2016, IEEE standard for local and metropolitan area networks — part 11: Wireless LAN medium access control (MAC) and physical layer (PHY) specifications," Jun. 2016, http://standards.ieee.org/.

[22] H. Yu and T. Kim, "Beamforming transmission in IEEE 802.11ac under time-varying channels," *The Scientific World J.*, vol. 2014, pp. 1–11, Jul. 2014, article ID 920937.

[23] M. Mathie, "Monitoring and interpreting human movement patterns using a triaxial accelerometer," Ph.D. dissertation, The University of New South Wales, Aug. 2003.

[24] D. P. Kingma and J. Ba, "Adam: A method for stochastic optimization," *arXiv preprint*, pp. 1–15, 2014, https://arxiv.org/abs/1412.6980.

[25] N. Srivastava, G. Hinton, A. Krizhevsky *et al.*, "Dropout: A simple way to prevent neural networks from overfitting," *J. Machine Learning Research*, vol. 15, pp. 1929–1958, Jun. 2014.

[26] L. Prechelt, "Automatic early stopping using cross validation: Quantifying the criteria," *Neural Networks*, vol. 11, no. 4, pp. 761–767, Jun. 1998.